AAS-07-430

FREE FLYING EXTERNAL OCCULTER MISSION DESIGN, SIMULATION, AND ANALYSIS

Ian J. E. Jordan[∞]

ABSTRACT

This presentation encompasses mission design, computer simulations, methods, and analysis of free-flying external occulter space astronomy missions with focus on traverse modeling and simulation of a likely range of 1-AU fallaway and E-S L2 terrestrial planet finder class vehicles. A theoretical model relating critical mission parameters will be contrasted with computer simulated traverses. The model constraints will be discussed in context of meeting critical science criteria for completeness of surveys around target stars. Discussion of the model implementation for single and multiple occulters and its extensibility to future applications will be highlighted.

ORGANIZATION OF THIS PAPER

After an introduction to the concept of external occulter space science missions, the roadmap for this paper is as follows:

- a brief review of known external occulter mission modeling and simulation,
- a derivation and justification for a statistical-dynamic-like scaling model that can be used for quick evaluation of external occulter missions,
- discussion of the constraints and strategies used in occulter missions, and
- description and preliminary results from simulation of a few external occulter missions.

This paper concludes with a brief recap, roadmap for future work, acknowledgements, notation, and references.

INTRODUCTION

External occultation is an astronomical technique that allows close companions to be spatially resolved and observed. Naturally occurring occultations have long been used for selenodetic and lunar orbit refinement purposes, as well as a means for probing atmospheres, sizes, and orbits of other bodies within our own solar system. Internal occultation at the focal-plane (coronography) was developed by Lyot in the 1930s (Ref. 1) for solar coronal observations and has been extended to the study of faint stellar companions (Ref. 2, 3). An early description of artificial external occultation for use with telescopic extrasolar planet studies was given by Spitzer (Ref. 4) and attributed to Danielson. Due to the great distances of stars, the

[∞] Scientist with Computer Sciences Corporation, functionally performing HST science planning and software development, and conducting research at the Space Telescope Science Institute, Operations & Engineering Division, Science Mission Scheduling Branch, Long Range Planning Group; 3700 San Martin Drive, Baltimore, MD 21218. Contact: Jordan@stsci.edu, 410-338-5037, http://www.stsci.edu/~jordan .

tiny angular separations of planets from them, and the large contrast ratios involved, the technique requires extremely large scales for external occulter designs (Ref. 5, 6, 7). Internal coronagraphs are fast approaching maturity for studying jovian-like extrasolar planets--and in principle earth-like ones as well (Ref. 8, 9). However, terrestrial-analogues are magnitudes fainter than jovians and closer to their parent luminaries, forcing stringent system requirements and making the external occulter cost an attractive alternative in the search for and study of earth-like planets around the nearest stars (Ref. 10).

Resurgent interest in external occulters after ranking low in the Terrestrial Planet Finder (TPF) Architecture Reviews (Ref. 11) has occurred in no small part due to recognition of the effectiveness of binary screen designs, known as early as Spitzer (Ref. 4), extolled by Marchal (Ref. 6), investigated by Starkman & Copi (Ref. 12), and championed by Cash (Ref. 13, 14). These screen concepts employ petal-like edges that function as a narrow-angle nuller of diffracted starlight. The binary screen creates a deep shadow broad enough to be occupied by a telescope at great distance, enabling the potential for simultaneous astrometry, photometry, and atmospheric spectroscopy of terrestrial-analogues at sub-arcsecond separations from their parent stars.

The only external occulter space science missions flown to date have been numerous solar coronagraphs (e.g., Ref. 15, 16). The prime enabler of solar-coronal, structurally connected, occulter-telescope configurations is that the occulting disk is greater than 0.5 degrees across and the telescope aperture need not be large. Exo-terrestrial analogues are many orders of magnitude fainter than solar coronal features, so telescopes many meters in size are necessary. Due to the tiny angular separations of extrasolar planets from their stars, the required separations of tens of thousands of kilometers prohibits structural connectedness of the telescope and occulter. External occulter architectures inherently have two significant constraints impacting their mission design compared to other architectures in the context of this type of science mission: long vehicle transit times between targets, and sun-angle viewing restrictions. For a non-trivial science program competing in scope with internal coronographic techniques, many target stars must be surveyed--mandating system ‘slewability’--with adequate target phase coverage.

Although some space-based screen system designs have entertained telescope mobility (Ref. 17), the greatest focus is on mobile occulters (Ref. 7, 18) for science efficiency and quality reasons. Regardless, transit requirements in the space environment coupled with science requirements impose constraints that form the basic boundaries for treatment in the present work. The concept introduction here is necessarily brief, and interested readers are urged to conduct internet searches on the terms ‘external occulter’, ‘star visor’, or ‘starshade’, or visit a few URLs in the references (Ref. 19) for more illustrative descriptions.

OCCULTER SCIENCE MISSION MODELLING

Science requirements drive space mission architectures and constrain mission designs. The domain of external occulter planet-study missions has typically been cast under the mantle of the TPF concept (Ref. 20). However, the goal of finding terrestrial planets is tightly coupled with their subsequent study since in order to state that one has found a planet with some degree of similarity to earth, it must be discriminated from other possible objects such as faint stars, galaxies, and other planetary or circumstellar objects. In this context, the TPF problem expands into a more challenging one requiring astrometry for orbit characterization, photometry for analysis of object variability or rotation, and spectrometry for atmospheric and surface composition determination. The Kepler space mission will search for transits to determine orbital periods and sizes of such objects, but the other characteristics will remain speculative. The objects that Kepler may find are orders of magnitudes more distant than the nearest stars. Studying their surfaces or possible atmospheres by spatially resolving the planets from their parent stars must wait several generations of significant advances in the capability of astronomical instrumentation.

To study atmospheric composition of terrestrial-like planets, the tools of astronomers must turn to the brightest and nearest stars where electromagnetic signatures are strong enough and exoplanets are capable of being resolved from that of their parent stars. Interferometers, coronographic telescopes, and external occulter architectures have widely been recognized as providing pathways to these science goals.

Orchestration of the science observations in concert with the architectural limitations must be well understood in the mission design phase. Without reasonable understanding of architectural limitations and their effect on an optimum science program, assessing the trade-offs among different architectures cannot be done properly. The relevant analysis must be done well in advance of committing resources so that decisions among the many architecture options are made in the wisest way.

The current paper considers the balance between dynamical efficiency and science utility and comments on how science performance metrics can be used in the evaluation of external occulter missions. Detailed Monte Carlo simulations of mission completeness are not broached here. The focus is narrowed to mission scopes of interest to the TPF community as well as accommodating engineering constraints and assuming that other science programs may factor into observatory goals. A simple statistical model relating critical engineering and science architecture parameters is introduced, its predictions are examined, and a simulator using a version of the TPF target shortlist will be described.

Brief History of Relevant Science Mission Modeling

Various estimates of external occulter science capacity (defined here as number of targets and observations) have been discussed. Woodcock (Ref. 5) used simple dynamics of fuel consumption, range, thrust, and spacecraft mass to estimate observing capacity for chemical propulsion missions. He concluded that higher-specific impulse propulsion (e.g., solar-electric) was indicated for such missions. Copi and Starkman and the BOSS team drew similar conclusions in the mid- and late-1990s.

In 1998, the current author began exploring external occulter mission design with the UMBRAS group, adopting a statistical dynamic-like approach to estimating the relationship between critical mission parameters (Ref. 21). This simple analytical approach lends itself well to first-order mission capacity measures for external occulters. In 2003 (Ref. 22), basic mission scaling arguments were put forth on the general relationship between the number of occulters, target station separations, spacecraft subsystem mass budgets, and launcher-constraints. Although benefits of multiple occulters were previously understood, this was a preliminary quantitative step toward understanding practical scalability.

In 2004 (Ref. 23), results of the statistical dynamic model of continuous thrust transits were presented in the context of assisting TPF-C to meet its goals. A brief justification and derivation of the statistical dynamic model is given in the current paper for completeness, and is used in comparison with simulation results. Following up on this previous work, the analytical approach was expanded to include formation-keeping inefficiencies and was used algorithmically to map out consumables consumption for a broad occulter mission parameter space in an unpublished study. This approach is useful for quick mission scaling evaluation, but lacks sophistication of high fidelity simulations.

Although binary apodization of external occulters has been discovered numerous times, with the rediscovery and popularization of the binary apodized starflower in 2005, many institutions have taken a fresh look at external occulter mission designs. With an important increase in fidelity, computer simulation of 2-impulse and continuous thrust transits with repeat visits to the TPF-shortlist was implemented by D. Lindler of *Sigma Space Corporation* in 2005/6. Those simulations supported mission design for the New Worlds Discoverer proposal submitted in response to a NASA Discovery Mission RFP (Ref. 24). Sarah Hunyadi presented summary results of sequencing external occulter transits for the New Worlds Observer (Ref. 25) mission in 2006 as part of a JPL review of occulter capabilities for meeting TPF goals. Hunyadi examined occulter traverses for between 40 and 60 targets with a small subset of targets receiving a second reobservation. Levels of completeness were derived for particular mission profiles.[*]

Martin Lo separately examined a single external occulter operating with a telescope in a ~ 750,000 km radius Earth-Sun L2 (ESL2) Lissajous orbit (vertical amplitude ~187,000 km) as well as an earth-fallaway

[*] Note announcements for the San Diego SPIE conference, 2007-08-28: D. Lindler, "TPF-O design reference mission", SPIE 6687-33; S. L. Hunyadi, A. S. Lo, "Detecting and characterizing extra-solar Earth-like planets with two external occulters", SPIE 6693-02.

orbit employing high fidelity simulation of tidal effects upon traverses and formation-keeping requirements (Ref. 26). Targets used were subsamples of the TPF prime target list as well as randomly distributed targets. M. Lo noted the large variability of the tidal acceleration components depending upon location of the occulter-telescope within the chosen orbit. Significant differences between fuel requirements for the large-Lissajous orbits and earth-fallaway were quantified. Those studies looked at mission profiles that were typically 1-visit per star or used revisit-time constraints to derive propulsion system and wet-mass requirements rather than inversely (mission capability, given propulsion and mass constraints).

In 2007, Kolemen and Kasdin published analyses of transits for ESL2 orbiting external occulter missions. Kolemen (Ref. 27) studied the ESL2 topology of single occulter missions, discussed dynamical-optimization algorithms applied to 2-impluse and continuous thrust transit cases, and also laid a foundation for the analytic representation of weakly constrained approaches to occulter transit optimization. Additionally, Kolemen applied these ideas to simulations of single-visit surveys of the top-100 TPF candidates. In a related paper (Ref. 28), dual-occulter missions were treated starting from the same approaches. The Kolemen-Kasdin approach is particularly useful for cases where many occulters participate in a science mission and propellant usage is minimized in allowable ways.

The formal approach presented by Kolemen is useful in exploring the limits of the transit problem from a dynamical point of view. Science metrics are certainly to be levied by the broad scientific community to judge the merits and drawbacks of this mission type. The science capacity of space-based surveys is a focus of many in the context of the capability of the TPF missions (Ref. 29-34). The metrics measuring observational completeness, recovery and loss of candidates in revisits, and observational biasing are of concern for external occulters given the inherent architectural constraints. The scientific value of any TPF candidate mission may be called into question if its design does not adequately balance science performance against econometric measures such as dynamical efficiency.

RETARGETING CAPACITY: A STATISTICAL DYNAMIC MODEL

Mission design for distributed platforms must account for constraints imposed by kinematics, engineering considerations such as propulsion system characteristics, and science requirements such as target observation rates and science activity durations. Mission scope and capability may depend directly upon these factors, so a general relationship between mission capability and basic physical principles could guide mission designers when trade factors inevitably apply pressures to change the architecture in some way. A simple analytic model may be a useful tool in such analysis if appropriately calibratable.

In this section, a simple canonical model used for mission scaling purposes in older literature and mission studies is introduced. It is important to stress in advance that the model only applies in free space and has limited applicability for many ESL2 missions or missions where the occulter(s) is (are) underpowered relative to tidal forces that act to shear the formation. The consequences of this will be glimpsed in simulation results presented in a later section. In derivation of the model, a *platform* refers to a stationary spacecraft around which a *vehicle* moves from one station to another. The statistical nature of this model comes from assuming that the sites the vehicle visits are distributed uniformly on the surface of an imaginary sphere. For missions employing continuous thrust between target stations, it is then possible to derive statistical relationships between relevant spacecraft and mission design parameters.

A 'Flat Space' Approximation

In developing any statistical-dynamic model, the domain of validity must be established. In this case the model applies to vehicles moving about a stationary platform. If the environmental forces are greater than the control authority of the vehicle, then it may be difficult to develop general relationships. In this simple model (but not simulations discussed in later sections) inherent transit acceleration produced by the main propulsion system is required to be much greater than ambient forces on the vehicle (such as gravitational tides and solar radiation pressure) for continuous thrust missions. For near-term expected external occulter missions, this is likely to be the case. Quantification of the ambient accelerations is given

elsewhere (Ref. 35). For chemical propulsion missions that would use point-impulse transfers between target stations, the requirement can be expressed somewhat differently in that the delta-V of the transfer must be greater than the cumulative ambient delta-V, but this is not pursued here.

For the domain of external occulter astronomy missions, the environment this discussion covers includes particular Earth-Sun L2 (ESL2) orbits with occulter-telescope separations out to ~100,000 km, and earth-fallaway solar orbits. Propulsion systems such as the DS-1 XIPS gridded-ion thruster (Ref. 36) are capable of providing adequate authority to allow the flat-space approximation to be reasonable to low-order. It should also be understood that an "equals sign" in the derivation that follows may encompass several different types of caveats, and often should be interpreted as an approximation symbol.

Vehicle Kinematics Around a Stationary Platform

It is elementary to show that Eq. 1 relates the time duration of a vehicle continuously accelerating/decelerating between two inertially fixed stations, departing and arriving with negligible relative velocity. The quantity s is the separation between the two stations, and $T_{1\text{-}transit}$ is the total time of flight duration from departure to arrival. It assumes that turnover time plus departure and arrival activities are negligible compared to the duration of acceleration/deceleration. For purposes here, a better way to classify departure and arrival activities would be to include them with the time on station, $T_{1\text{-}station}$. This makes $T_{1\text{-}transit}$ a better estimate of the time spent in the translational phase between stations.

$$4s \cong a \cdot T_{1-transit}^2 \tag{1}$$

Eq. 2, forms the starting point of a relationship between station densities and the time needed to transit between them. The left-hand side of the equation expresses the average density of stations on a spherical surface of radius z, where n is the number of stations quasi-randomly distributed on that surface. On the right–hand side is the expected density of stations within distance s of any station where μ is the number of stations within this area, given that the direction of travel is restricted such that only a fraction q of all possible movement directions can be taken by the vehicle. More simply, the right-hand side expresses the density of targets in a pie-shaped area of radius s on the surface of the imaginary sphere. By equating left- and right-hand sides, areal densities are balanced for subsequent manipulation. This equivalence strictly holds only over small angles subtended from the sphere center, or equivalently for small patch areas on the sphere surface. For densities on the order of interest, it is an adequate approximation.

$$\frac{n}{4\pi \cdot z^2} \cong \frac{\mu}{\pi \cdot s^2 \cdot q} \tag{2}$$

If no restrictions are placed on the vehicle's direction of travel, then q=1. However, this will likely not apply for most missions of interest. Later, a case-study where the assumed value of q<=0.5 is discussed. On occasion, it is useful to refer to the ratio μ/q instead of just one of the two parameters. Historically, the author has used q=0.3 for mission capacity estimation, and this will be compared against simulation results.

Eq. 2 and Eq. 1 can be combined to yield a statistical estimate of the transit time between two stations out of n randomly located stations on a spherical surface as a function of the ratio of the operating range (station distance from sphere center) z to the acceleration/deceleration magnitude a (Eq. 3). Note that transit time scales as the square root of that ratio, and also scales inversely as the fourth root of the number of distinct stations given that μ is fixed.

$$T_{1-transit} \cong 2\sqrt{\left(\frac{2z}{a}\right) \cdot \sqrt{\frac{\mu}{nq}}} \tag{3}$$

If stations are not uniformly distributed, then the number within reach, μ, may be alternately interpreted as a function expressing the local variation from uniformity. Under such an interpretation, large values of μ (locally) are required to compensate for low global station densities, and vice-versa. Under this interpretation, μ is then not only a function of location on the surface relative to other stations, but depends upon s and q as well. If the stations can in some meaningful way be treated as uniformly or randomly distributed, then the case μ=1 is of interest by interpreting it as the domain where one expects a single station to lie in the accessible area encompassed within a distance s from another nearby station. In that case, one expects to transit to the next reachable station within the transit direction of regard.

Next introduced is a timing constraint prompted from science considerations. Consider the scenario of the vehicle visiting each station in a cyclic and exhaustive way, traveling to each of the n stations a number v times. At each stop, the vehicle spends a wait time of $T_{1\text{-}station}$ at each station. The total time to execute the v visits to the n different stations is given by Eq. 4. This relation is critical in computing propellant and propulsion requirements for time-limited missions.

$$T_{mission} = n \cdot v \cdot \left(T_{1-transit} + T_{1-station} \right) \tag{4}$$

Moving Point Dynamics: Changing Vehicle Mass

For a vehicle undergoing constant Newtonian acceleration produced by mass expulsion from the vehicle, the classical rocket equation applies. The ratio of the initial vehicle mass M_{init} to the final vehicle mass M_{final} is equal to a natural exponential (Eq. 5) of the ratio of the cumulative ΔV achieved and the mass expulsion (exhaust) velocity. In that relation, a is the magnitude of the acceleration, while the exhaust velocity is expressed as a product of I_{sp}, the propellant specific impulse (a standard engineering quantification of propellant and propulsion characteristics), and g, the gravitational acceleration at the earth's surface. The total time spent under acceleration is then T_{thrust}. .

$$\frac{M_{init}}{M_{final}} = e^{\frac{a \cdot T_{thrust}}{g \cdot I_{sp}}} . \tag{5}$$

Recognizing that the time expressed in Eq. 5 is approximately the same as the cumulative time spent transiting between all stations (Eq. 6) over the lifetime of the mission (ignoring formation-keeping propellant consumption for the time being), a simple sum can be stated:

$$T_{thrust} = T_{1-transit} \cdot n \cdot v . \tag{6}$$

Substituting Eq. 6 into Eq. 5 yields Eq. 7.

$$\ln\left(\frac{M_{init}}{M_{final}} \right) = \frac{a \cdot T_{thrust}}{g \cdot I_{sp}} = \frac{a \cdot T_{1-transit} \cdot n \cdot v}{g \cdot I_{sp}} . \tag{7}$$

Time-independent Parameter Relationships

Other constraints can be applied to eliminate variables and alternately characterize the trade space. If a mission designer wished to maintain constant acceleration in a mission, the thrust level must be throttled down as propellant is expelled from the vehicle since its mass continuously shrinks through mass expulsion. In such cases, maximum thrust F_{max} occurs when the vehicle is heaviest, M_{init}, which Eq. 8 relates to acceleration. Whether constant acceleration is optimal for the mission is a separate topic, and only constant acceleration mission profiles are considered in this derivation. For vehicles with small propellant mass fractions, this is a reasonable first approximation even for non-constant thrust missions.

$$F_{\max} = M_{init} \cdot a \tag{8}$$

Substituting Eq. 8 into Eq. 7 to explicitly eliminate acceleration, and substitution of Eq. 3 into Eq. 7 to remove explicit transit time dependence, yields Eq. 9. Here, initial and final vehicle masses have been isolated on the left of the equivalence and all the other variables on the right side with no explicit time dependency appearing. Unfortunately, this transcendental equation cannot be solved algebraically for propellant mass, although each of the other non-mass variables can be isolated.

$$\sqrt{M_{init}} \ln\left(\frac{M_{init}}{M_{final}}\right) \cong \frac{2n \cdot v}{g \cdot I_{sp}} \sqrt{2F_{\max} \cdot z \cdot \sqrt{\frac{\mu}{nq}}} \tag{9}$$

Isolating n in Eq. 9 shows how the number of surveyable targets varies directly as a function of the other dynamical and mission variables (Eq. 10).

$$n^3 \cong \left(\frac{q}{64\mu}\right)\left[\left(\frac{I_{sp} \cdot g}{v} \cdot \ln\left(\frac{M_{init}}{M_{final}}\right)\right)^2 \cdot \frac{M_{init}}{z \cdot F_{\max}}\right]^2 \tag{10}$$

Upon further flattening, the relation appears thus:

$$64\mu\, n^3 z^2 v^4 F_{\max}^2 \cong q \cdot M_{init}^2 \left[\left(g \cdot I_{sp}\right) \cdot \ln\left(\frac{M_{init}}{M_{final}}\right)\right]^4 \tag{11}$$

In Eq. 11, note the pair-wise dependency of the four variables, n, v, z, and F_{max}. These variables couple as to form inverse power dependencies. If any single one of these mission parameters increases in magnitude--without independently changing other mission parameters--then one or more of the other three must decrease correspondingly. It is interesting to note that the number of targets and the number of visits do not emerge symmetrically with respect to their functional relationship to one another. The number of visits per target appears at a higher power exponent than does the number of targets.

With Eq. 11, the derivation has arrived at a general time-independent relation among vehicle mass, propulsion system properties, vehicle-platform separation, plus number and density of stations for statistically distributed stations on a spherical surface. The other parameters included may indeed be functions of these and other variables, however their scaling characteristics will not be further discussed here and is left to interested investigators. Equation 11 may be regarded as a fundamental occulter mission scaling relationship.

Mission Duration Constraints

If mission duration is a constraint, then an additional relationship can be used to further characterize the parameter space. Equation 12 expresses the simple 'gas tank' relation with other estimable time and target mission parameters, discussed earlier.

$$M_p = \frac{F_{\max}}{g \cdot I_{sp}} \cdot T_{thrust} = \frac{F_{\max}}{g \cdot I_{sp}} \cdot \left(T_{mission} - n \cdot v \cdot T_{1-station}\right) \tag{12}$$

From this, eliminating acceleration with Eq. 3 through appropriate use of Eq. 8, and then substituting into Eq. 4, yields Eq. 13, expressing mission duration as a function of other mission parameters.

$$T_{mission} \cong n \cdot \nu \cdot \left(T_{1-station} + \sqrt{\left(\frac{M_{init} \cdot z}{F_{\max}} \right)} \cdot \sqrt{\frac{64\mu}{nq}} \right) \tag{13}$$

Case Study: Application to an Occulter Mission

Although the forgoing development is applicable to any space mission requiring mobile vehicles around stationary platforms, in this subsection it is applied to a single occulter moving between the spherically distributed stations such that the stations are positioned appropriately between the telescope and targets of interest. Because stars are at such great distances and their proper motions are relatively small, the stellar frame can be treated as inertial with respect to the local standard of rest for the duration of observations. Later, changing the value of a number of variables is used to explore the impact on other quantities, thus forming the trade space for telescope-occulter missions.

Missions where z is large enough to require a significant fraction of the vehicle's mass be constituted of propellant can and do result in limits for total mission duration ($T_{mission}$), mean visit duration at each station ($T_{1\text{-}station}$), and average number of revisits to each station (ν). Considering missions where the vehicle's acceleration level is constant (thrust is varied with the changing mass of the vehicle), a mission feasibility relation can be derived (not explored further here). The current case study will involve a mission employing a single large occulter operating at 75,000 km from a telescope. Although flight-proven gridded-ion systems have demonstrated I_{sp} greater than 3000 seconds, here an average of 2500 seconds over the total propellant load is used to allow for expenditure of formation-keeping fuel at an I_{sp} of only ~ 300 seconds. Arriving at this correction requires some iterative analysis that will not be discussed here.

ν = 3	M_{init} = 3000 kg
z = 75,000 km	M_{final} = 2500 kg
$T_{1\text{-station}}$ = 2 days	F_{max} = 90 mN
q = 0.3	I_{sp} = 2500 seconds
ρ = 1.3	

***Table 1**: Assumed mission parameters used in the example study.*

In Table 1, some likely possible mission and spacecraft parameters for a TPF-class occulter mission are given and used in this case study. If Eq. 13 is solved for n, with substitution of values from Table 1, and propellant mass is factored out as an independent variable, and then n is plotted as a function of propellant mass, the result is Figure 1 (where P = M_p). It shows the number of targets that can be surveyed with a given propellant load, assuming the constant acceleration profile discussed earlier. Another simple result is plotted in Figure 2, showing the relationship between propellant load and mission duration.

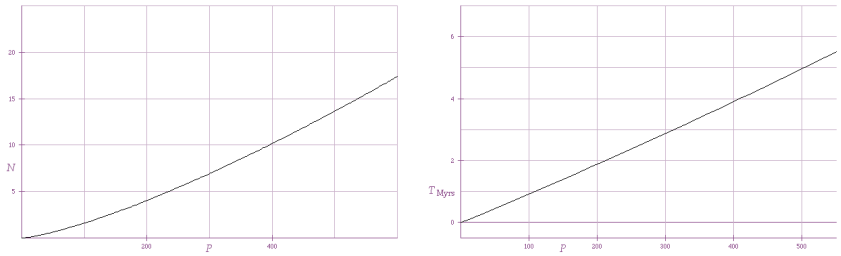

***Figures 1 (L) & 2 (R)**: Predictions by the statistical-dynamic model for the number of surveyable targets and mission duration as a function of transit propellant (kg) given assumptions in Table 1.*

Single Occulter Trade Space

Science and mission planners have a host of questions regarding tradeoffs between science quality and quantity factors, and the engineering and mission limitations. Suppose, for example, a mission planner wanted to know the mean number of distinct stations or targets surveyable and mission duration if the operating range was increased to 100,000 km. To compute the average number of stations, note from Eq. 13 that n is proportional to the inverse two-thirds power of the operating range when other mission parameters (ρ, q, v, F_{max}, I_{sp}, and M_{init}) are held constant. By increasing the operating range 33%, the number of targets then changes by a factor of $(4/3)^{(-2/3)} \sim (5/6)$. Instead of ~ 14 targets originally surveyed with three visits to each during 5 years, only ~12 targets could be observed with three visits to each. The relationship plotted for a wide range of separations is shown in Figure 3.

How long would the mission would take, assuming acceleration, maximum thrust, and total thrust time do not change? The cumulative time spent on station is the only phase with a different duration. Since 3 visits to each of 2 targets have been removed, the overall mission duration has been trimmed by 21 weeks. However, if the maximum acceleration were reduced to maintain the ability to observe 14 targets with 3 visits, then the mission length would increase. Figure 4 shows the relationship given that number of targets and visits per target are fixed quantities.

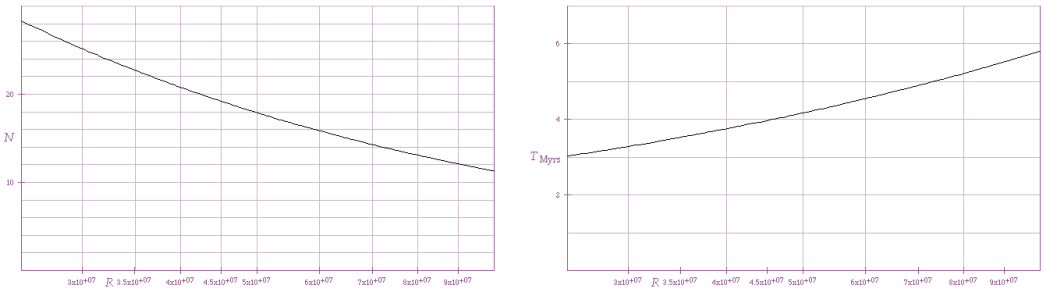

***Figure 3 (L) & 4 (R)**: Number of targets that can be observed as a function of altering the platform-vehicle separation. A fixed propellant quantity of 500 kg is assumed. Figure 4: Mission length (in years) is plotted as a function of platform-vehicle separation for 14 targets/3 visits each.*

A realistic possibility for an in-flight mission change would be that some subset of targets would become interesting candidates for re-observation, and would have their number of visits boosted. Without some change to some other mission parameter (such as total number of targets), this would not be possible. If the total number of targets were reduced, then the additional visits could be accommodated. If the average number of visits to a target were 4 instead of 3, then the number of unique targets that could be surveyed would be (14 targets) * $(4/3)^{(-4/3)} \sim 9.5$ targets. Note that with more targets/visit, the result is not only fewer targets, but also fewer total transits.

Another question of interest is how propulsion system changes affect the mission. Suppose one option allowed for 3000s specific impulse instead of 2500s. The number of targets could be increased from 14 to $14*(3000/2500)^{(4/3)} \sim 18$ or—of interest to the project scientist--the maximum operating range could be increased from 75,000 to ~ 108,000 km ($z \sim I_{sp}^2$) while maintaining the number of targets surveyable over the mission. However, this does increase mission duration to almost 6 years. Determining mission characteristics that scale back within a 5-year mission duration is left as an exercise.

Yet another interesting question arises if one asks, “what if the thrust level were reduced from 90 to 70 mN? What effect would that have on number of achievable targets and total mission duration? The number of targets that could be observed would increase to $14*(70/90)^{(-2/3)} \sim 16.5$. More than 2 weeks would be added to ‘station time’, while the time spent under acceleration would change according to the lowered mass expulsion rate (assuming that I_{sp} does not also change), increasing the total transit time by

28%. The net effect would be for the mission duration to stretch from approximately 5 years to approximately 6.5 years.

CONSIDERATIONS IN ADVANCE OF SIMULATION

Optimized Target Revisit Times

Studies by other groups indicate that the optimal revisit time between two TPF observations varies in complex ways depending upon the search goals and range of orbits of interest. In one study (Ref. 32), a TPF-C class system capable of an inner working angle (zone of obscuration) of 63 milliarcseconds observing a sun-like star at 10 parsecs was considered. The optimal revisit time yielding the greatest chance to observe an object from an ensemble of possible orbits in a hypothetical habitable zone around the star that were previously unobservable due to a central obscuration (coronagraph or occulter) is close to 70 days. However, that probability distribution is highly peaked and one of the least optimal viewing times occurs 6-months after the initial observation. After an optimally timed revisit, if again no object were observed, the optimal revisit time to increase the completeness of the survey for a third observation would be 3 months. Arenberg, et.al. classified the probability profiles versus time that concerned revisit reacquisition of terrestrial analogues and found several broad classes of behaviour. These categories were largely functions of proximity to the central obscuration of the moving target and its specific orbital parameters. Independently, Brown (Ref. 30, 31) found comparable revisit times are required in order to maximize completeness of a survey given that no candidate objects are detected in an initial observation.

The desire to obtain astrometry adequate to characterize orbital parameters of any detected moving target influences choice of revisit times since multiple observations are required to compute an orbit. Brown (Ref. 37) has also pointed out that disambiguation of moving targets from background sources such as galaxies and stars requires carefully timed revisits. This is most critically the case for the faintest targets near the detection limit. Stellar proper motion and parallax combine to produce optimal and sub-optimal observing seasons in TPF missions when considering ensembles of planet candidates placed around the best nearby candidates. However, reobservation prompted by disambiguation requirements may be mitigated to some degree (except for the faintest targets near the detection limit) by performing low-resolution (R~5) spectrophotometry on the field targets, as suggested by others (although this does not solve the problem of orbit determination). The crucial point is that planetary objects have different color-color signatures than do likely field-stars and background galaxies as viewed in visible wavelength filter-bands. In the context of an external occulter, this allows single visits to provide discrimination of planetary companions from other faint objects, thereby yielding input into future observing sequence planning.

In ESL2 halo-orbit occulter missions, the sun-tide is typically manageable for executing transits, but the earth tide can be significant and possibly swamp the authority of the primary transit engine if the mission is relatively underpowered. For example, in a slightly inclined halo orbit with a radius of 500,000 km, the earth-tide varies by a factor of ~ 8. It is about 4-times the magnitude at closest earth approach than at ecliptic-plane crossing. At this juncture, it is worth proposing a scheme that offers mitigation of earth-tide issues for ESL2 telescope-occulter missions: smaller halo orbits. Such smaller orbits have been avoided for science mission planning in the past largely because of two issues: communications difficulties, and power and thermal stability concerns from eclipses.

Inclined halo orbits avoid these problems, however lunar eclipses are not excluded unless the halo orbit radius is greater than about 400,000 km. Nevertheless, halo orbits smaller than 400,000 km yield eclipses that only involve illumination drops with amplitudes of about 6% and durations of about half an hour in the case of a 250,000 km radius halo orbit at moderate inclination. An ESL2 spacecraft in that orbit would only be in the eclipse band less than 1% of time (less than a day at each crossing), and the random likelihood of the moon casting a shadow on that segment of the orbit is less than 10%. Resulting expectations are that a lunar eclipse would occur about once every 5 years. In the event of a predicted mutual crossing, a 1-m/s course adjustment 1-2 months in advance could avert the lunar eclipse. This is several times the stationkeeping requirement for halo orbit maintenance during such an event, but likely

acceptable given the rarity—particularly if it reduces the constraints on target sequencing for the occulter. Shrinking the halo radius may not provide substantial benefits for single spacecraft missions (such as JWST or Hershel), but missions requiring formation flight near ESL2 should evaluate this option.

Occulter Usage Strategies

External occulters can usefully provide revisit times 6-months apart, although single-occulter missions incur great inefficiencies because the occulter may need to 'hop' from one side of the quadrature ring to the other in order to obtain a 6-month observation spacing on the target star. However, intervals of 2-3 months are not generally favorable spacings in single external occulter missions because (for stars near the ecliptic) this requires visits that occur as the star enters and as it is about to leave the quadrature ring. This entails 'backtracking' by the occulter and while useful for particular target stars, such a strategy is not optimal globally since opportunities to observe other stars passing through the quadrature ring will be missed. Missing these observing opportunities generally increases the average transit distance required, decreasing the overall efficiency of the science mission.

If the occulter is designed such that the quadrature ring is very narrow, then such observational spacing cannot be achieved during a single year. Instead, sampling of the phase space of possible exoplanetary orbits must be done over the course of an external occulter mission that spans a number of years. Because external occulters have significant slew and field-of-regard constraints, asserting primacy of the optimal revisit times might overconstrain the mission and decrease its observing efficiency. Instead, weighting the optimal revisit benefits against external occulter traverse and target sequencing issues must be confronted (but not here).

Dualing Occulters

If an external-occulter mission employs more than one occulter, then new sequencing strategies become possible. To understand these strategies better, one may consider a few extreme cases. These cases assume a strong desire to perform reobservation of the target stars within a period of one year.

Follower-leader: In this strategy, the occulters generally stay on the same side of the quadrature ring, with one occulter following behind the other. The first occulter is used to observe target stars as they enter the quadrature ring, while the second is used just before the star exits. An advantage of this approach is that the smallest time-spacings between follow-up revisits can be employed without sacrificing efficiency of movement by either occulter. However, one disadvantage is that unless the flotilla of two executes a circumnavigation of the quadrature ring at a frequency of 1-year, revisiting the target star six-months after the initial observations is inefficient from a fuel and time standpoints.

Opposing occulters: Here, the general concept is that the occulters maintain general locations on opposite sides of the sky (as viewed from the telescope), operating in a way that target stars are re-observed 5-7 months after previous observations. There is a mission efficiency gain in that long occulter slews to the opposite side of the quadrature ring are not required for the half-year interval reobservation of a particular star. However, the downside is that the short-interval reobservations of 2-3 months can only be performed with the backtracking penalty.

In an actual two-occulter mission, it is unlikely that either one of these extreme examples of mission sequencing would be adopted The assumption of needing to perform all observations on the targets within a 1-year period may be overly restrictive in the context of the scientific potential of each target. In a real occulter mission, the detailed knowledge of the target stars' environments will change priorities for the needed reobservation times. This will then alter the sequencing and pure forms of these strategies would dissonantly break down. Studies of the science benefits of compact versus longer-baseline distribution of observations for TPF purposes suggest that the longer baseline has some scientific advantages (Ref. 34).

Earth-Sun L2 Tides

Opposing occulter strategies circum-ESL2 can be difficult to orchestrate if the craft are underpowered with respect to the Earth-tide. This can be understood by imagining an occulter craft near the ecliptic plane with respect to the telescope and located at greater than a 90-degree earth-telescope-occulter angle. The occulter is 'pulled' or sheared by the tide toward the anti-earth (with respect to the telescope) with an acceleration component amplitude that increases as the telescope-occulter line increases beyond 90-degrees with respect to the Earth. This can be beneficial for occulters making anti-earthward transits on the trailing side of the telescope relative to the general orbital motion around the sun. However, this configuration imposes a 'tidal hill' that an occulter must climb for earthward transits. Earthward transits on the lead side of the telescope are important for most circum-ESL2 occulter missions because this is also in the general direction in which the quadrature ring rotates, and occulters are most efficiently used if targets can be queued to take advantage of their entry and exit at convenient times.

In an opposite sense, if the earth-angle is lower than 90-degrees, the occulter is pulled toward the earth relative to the telescope. In manner opposite to the previous case, this is beneficial for occulter transits being made earthward, particularly on the lead-side of the quadrature ring. However, if the occulter trails the telescope in orbit around the sun, the occulter must climb 'uphill' to reach targets that are nearby.

More than Two Occulters

Once an external occulter mission has three external coronographic vehicles, then a pure form that combines both follower-leader and opposing-occulters would be possible, combining the desirable aspects of both and avoiding the undesirable ramification of either. Four occulters offer an opportunity to use both strategies on both sides of the quadrature ring (leading and following the telescope's sun-orbital motion). Benefits of occulter constellations (Ref. 22) and the orbital dynamics have been explored in some depth by Kolemen (Ref. 28), and will not be considered further here.

OCCULTER MISSION SIMULATION

Mission simulation provides higher-fidelity result than a simple analytical model can hope to encompass. Simulation must be applied to incorporate diverse aspects such as uneven target distribution, actual field-of-regard issues, varying transit profiles, unequal optimum revisit times and on-station times for different targets, and the effects of geometry and environmental factors on the transit kinematics.

Many approaches to building an occulter mission simulator are possible. Factors influencing the choice are diverse, encompassing issues such as mission architecture (e.g., how many occulters?), is the mission dedicated to optimizing external occulter science or is it just one component of a larger science program? Should one take an existing mission simulation tool for a space-telescope science mission and adapt it for use or should a tool be built from scratch?

This author's choice of computer language for implementation fell in favor of a rapid prototyping environment. For the current study, an interpreted, Python-based, functional programming toolset mixed with some objected-oriented entities and an extensive public-domain set of libraries formed a toolkit for development of an external occulter mission simulator in a UNIX environment. On a laptop computer running at 400 MHz, simulation times (with day-long time steps) spanned from a few minutes to a significant fraction of an hour depending upon constraint and modeling fidelity, mission duration, and level of automated post-simulation analysis. The simulator operates on a user-input target-list and approximately 25 architecture and mission parameters. These user-specified parameters included number of occulters, telescope-occulter operating range, earth-telescope and sun-telescope range (plus orbit-class parameters), sun-angle restrictions for target selection and sequencing, mission start-time, mission duration, maximum occulter transit and formation-keeping thrust levels, midcourse turnover-duration, primary and formation-keeping propellant quantities and I_{sp}s, time-on-target rules, simulation time-step, and survey-mode revisitation rules.

In addition to adapting the rules and algorithms to accommodate mission parameters, and simulate transits, tools for analysis of science quality consequences were developed. Some techniques outlined by Brown and Arenberg have been implemented, but the extensive Monte-Carlo approach has not yet been adapted into the simulator capabilities. Science quality analysis within the simulator is still in the early stages of development and not discussed extensively here. Target selection algorithms are a critical scientific issue, and will form the cornerstone of great attention if external occulter missions are approved.

Information about individual star systems will be important factors in determining re-visit strategy and priority for a target star. For example, many star systems will show exo-zodiacal dust and debris disks. Knowledge of their orientation, brightness, and inclination of the disk with respect to our vantage point are important for interpreting whether observed exoplanet candidates are likely background sources, distant or close-orbiting planets, and gauging their likely orbital inclinations--depending upon observed brightness and color characteristics. This information is also important input for choosing the preferred timescale for revisits to the target star, and estimated levels of completeness.

Some Architecture Constraints Avoided

Other mission simulation constraints need to be considered. Earth- and moon-shine avoidance zones may be required depending upon the reflective characteristics of the occulter screen and operations issues—a reflection of the earth or moon by the occulter into the telescope could compromise science. Occulter tilt may be adjusted operationally to mitigate this problem and remove it from the simulation domain. For earth-fallaway orbits, an earth/moon-avoidance zone for the target-telescope line of sight versus time is needed for highest fidelity.

Also important in power-limited, solar-electric propulsion missions is power available for the acceleration and deceleration legs of each transit. Some occulter architectures could have the solar arrays blocked from sun illumination on either the acceleration or deceleration legs of particular types of transits, notably those that parallel the sun-antisun direction. The larger the screen and closer the solar array lies to its center, the more restrictive this becomes. This can be a significant constrainer of architecture choices, and the ‘central unibody’ (without design redundancy) occulters tend to suffer this affliction, while ‘flyswatter’ or ‘pinwheel’ architectures provide a greater degree of immunity from this problem (Ref. 38).

The simulations presented here do not use these reflection and power restrictions for candidate selection. The goal instead is to demonstrate the basic capability of the simulator. As has been noted, particular mission constraints other than these have a significant impact on outcomes and the ones presented here are only representative of the broad characteristics of occulter missions.

Simulation Scope

Currently, several simulation cases are contrasted for 5-year telescope-occulter missions having nominal telescope-occulter separations of 75,000 km. The field of regard for telescope-occulter observations is assumed centered on the quadrature ring with a half-width of 20 degrees. All simulations discussed here have traverses among the top 35 TPF candidate stars (Ref. 31) except for the single occulter, earth-fallaway orbit where 20 and 35 target selections are simulated and contrasted against each other.

- single occulter mission, earth-fallaway orbit
- double occulter mission, earth-fallaway orbit
- double occulter mission, ESL2 halo orbit.

From spacecraft operations and science mission perspectives, fuel and time are resources that must be traded off against optimal observing sequences. Transit times computed by the algorithm accommodated any ‘wait time’ needed until a target was within the field of regard (in the quadrature ring), and adjusted the transit thrust downward to appropriately match the transit duration. The target selection algorithm picked

for these simulations was based upon several very simple rules with the fundamental metric representing spacecraft resources (i.e., transit fuel and mission time) that embodied a simplistic, 'greedy' algorithm:

- Candidate selection favored minimum transit time and propellant usage.
- No target revisit was allowed within 50 days times the luminosity-scaled period of a 1-sol illuminated circular orbit.
- Candidates with 3 or more observations incurred power-law penalties in proportion to the number of previous observations.

The uniformity of the distribution of the observations and the relative uniformity in sampling planetary orbits with varying periods are measured during simulations. As implied by the work of other researchers, a particular pattern of non-uniform sampling may provide superior completeness. Displayed in the figures that follow are phase data relative to the first observation on each target for a presumed planet in an orbit which would correspond to 1-sol illumination (~1365 W/m^2—that at Earth) in order to point out the asymmetry in phase coverage and patterns that result from employing the simple candidate selection algorithm.

These simulations assume traverse profiles that are 'search-dominated' from a science productivity standpoint. Such occulter observations do not typically spend more than a few days on-target because objects of interest do not require significant amounts of observing time to reach the 'candidate-discovery' threshold, or their orbits are not well defined enough for extended-stay revisits to be planned with enough certainty to ensure that the objects of interest will not be hidden behind the occulter. Since the frequency of occurrence of terrestrial-analogues around particular stars is not yet predictable, this assumption yields simulations that are compact in duration. Use of a single set of rules for candidate selection with no expectation of sequence changes during the mission will not match circumstances in a real mission. Discoveries made by observations of the target stars will prompt sequence replanning with great frequency.

Single Occulter, 20 Target Sample versus Single Occulter 35 Target Sample

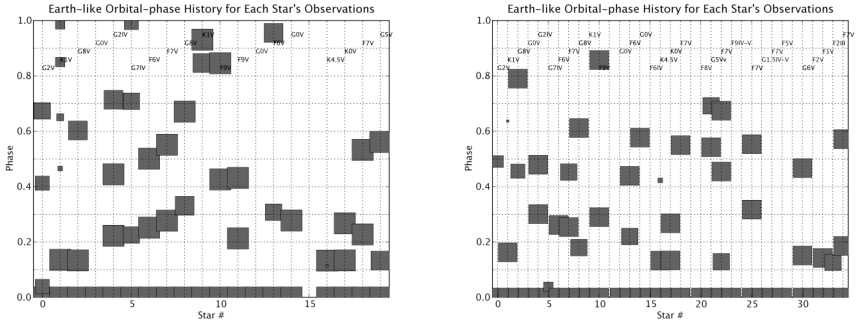

Figures 5 (L) & 6 (R): *The relative-phase-of-observations in two single-occulter missions (as described in the text) for a hypothetical extrasolar planet around each observed star whose orbital period corresponds to 1-sol illumination. Sizes of the squares indicate the integer phase of an observation (i.e., whether it would occur in plan-orbit 0, 1, 2, etc.), with smaller squares indicating observations occurring during later 'extrasolar orbits'. On the left, the occulter mission used only a 20 target subsample from the TPF shortlist, and on the right is displayed a mission simulation that used 35 targets. Stellar spectral type is printed above the corresponding column of observations for each star, underscoring that each target star has habitable zone orbits with their own intrinsic period.*

Figures 5-10 summarize and contrast occulter sequencing to 20 and 35 target subsets using the simple algorithm outlined above. It bears pointing out here that the simulations show approximately 20 targets can be observed on average 3 times during the mission. Note that this is better than the prediction of the statistical-dynamic model presented in an earlier section. In examining the detailed occulter traverses, this

appears to be due to the fact that a very conservative estimate of 'q' was used in the model case study. Choice of 'q' and 'μ' in that section was made specifically to illustrate that historical estimates arrived at in previous mission capacity estimates are more conservative than those arrived at in the simulations presented in this section.

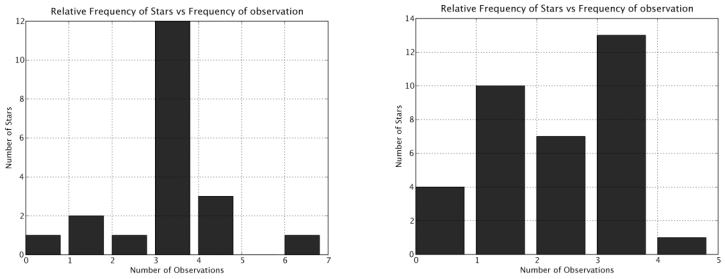

Figures 7 (L) & 8 (R): *Distribution of number of stars with the given number of telescope-occulter observations for the two simulations described for Figures 5 (20 target subsample) & 6 (35 target subsample).*

Figures 5 & 6 indicate subtle differences in the 1-sol observation phasing across the subsample of stars. The 35-target sample allowed 67 observations in the 5-year interval, but only 58 observations were possible in the 20-target sample. In this 20-target case, the fraction of the follow-up observations on the target stars at phases between 0.0 and 0.5 was approximately the same as phase range 0.5-1.0. Interestingly, for the 35-target sample, more than twice as many reobservations were conducted at the phase range 0-0.5 as in 0.5-1.0. Note that the phasing plot shows a few targets which had observations spanning a significant number of orbits by the planet around the star.

As shown in Figures 7 & 8, the different distributions of stars per observation count is a direct result of one sample being tuned to reach the 3-observation goal while the other was not. The time-greedy target selection algorithm allowed some targets to remain underobserved even in the 20-target subsample because penalties for above-3 observations were not severe enough to mitigate it.

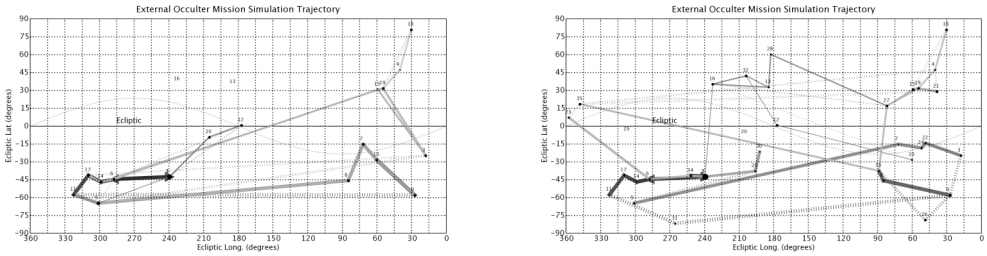

Figures 9 (L) and 10 (R): *Occulter traverse sequencing history for the 20-target and 35-target subsamples corresponding to the single occulter simulations presented in Figures 5-8, and plotted in ecliptic coordinates. Transits of earlier observations in the mission are delimited by broader lines, and dashed lines show transits where the ecliptic longitude wrapped beyond the 360/0-degree boundary. The lines do not represent the actual occulter track on the sky. The number tagged with each target star corresponds to the numbering in Figures 5 & 6 (plus a 1-count offset). Rightward pointing triangles mark the starting occulter location; leftward pointing triangles denote the mission completion location. Mission start time (all simulations) is January 1, 2015.*

Dual Occulters, 35 Target Samples: Earth-fallaway versus ESL2 Mini-halo

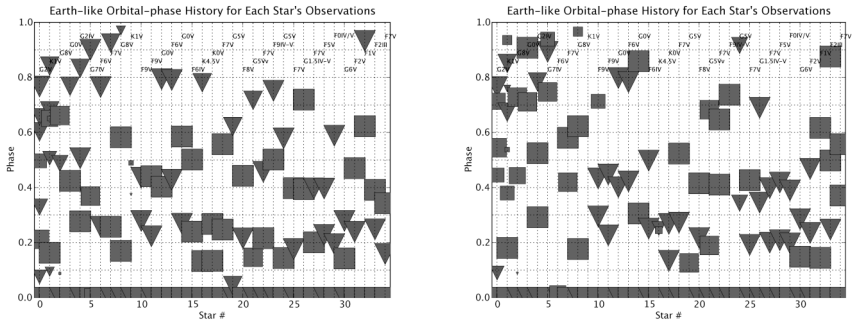

Figures 11 (L) & 12 (R) 1-sol illumination phase distribution plots for 35 star subsamples in dual-occulter fallaway (L) and ESL2 (R) missions. 'Occulter 1' is denoted with squares, 'occulter 2' with triangles.

For the dual occulter, fallaway, 35-target sample, 119 combined observations were conducted. In spite of the completeness level of 3-observations per star, similar to the 20-observation, single occulter case, the phase distribution (Figures 11 & 12) of the observations had greater similarity to the 35-target single occulter case—almost 65% of the reobservations were between phases 0-0.5. If we compare this with the 2-occulter ESL2 case, 114 observations were conducted, with 60% of the reobservations between phases 0-0.5. Both scenarios had good ability to meet the minimum 3-obsservation goal (but reduced earth-tide magnitudes made the task more achievable) as seen in Figures 13 & 14.

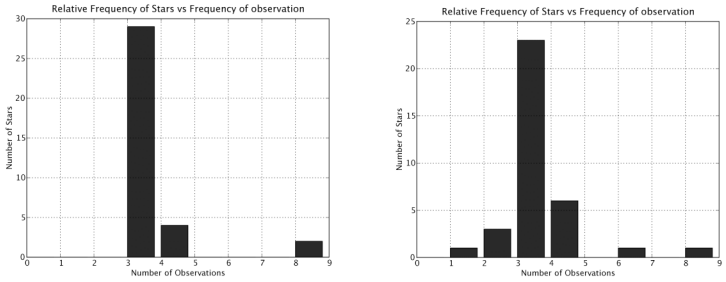

Figures 13 (L) & 14 (R): frequency of stars with given number of observations for the 35 targets in each of the two occulter missions: fallaway (L), and 250,000 km radius halo orbit at ESL2 (R).

Common patterns in the transit sequencing can be seen among all of the simulations shown here. This is a natural consequence of their common target selection algorithm, however the differences seen in the sequencing diagrams are illustrative of the fundamental differences between the scenarios. For the dual-occulter mission comparison, the occulters tend to execute pair-wise-similar tracks during certain phases of the traverses, as seen in Figures 15-18. However, the occulters clearly have greater difficulty selecting certain targets due to the Earth-tide effects. Some of the 'backtracking' that is performed in the fallaway case does not materialize for the ESL2 halo orbit. Consequently, some individual targets are not sequenced efficiently with the greedy algorithm, and the total number of target visitations drops and the sequencing patterns change. This distinction becomes more pronounced with ESL2 orbits with closer approaches to Earth or with occulters that have lower transit authority relative to the tides.

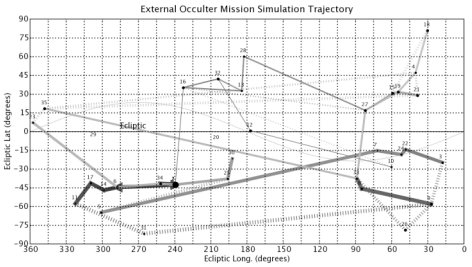

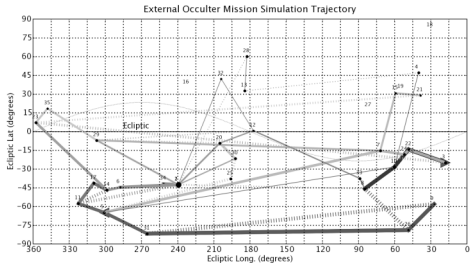

Figures 15 (L) & 16 (R): Traverse sequencing of the individual occulters in the Earth-fallaway orbit mission.

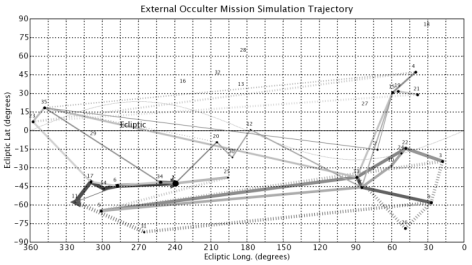

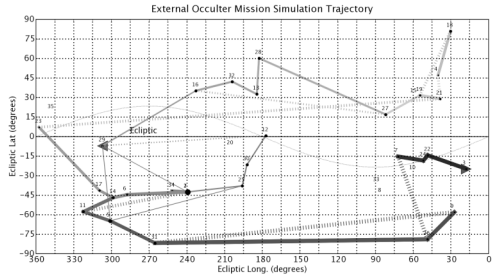

Figures 17 (L) & 18 (R): Traverse sequencing of the individual occulters in the 250,000km radius halo orbit ESL2 mission.

CONCLUSION & RECOMMENDATIONS

Differences exist between previous mission capacity estimates derived from the statistical dynamic model and numerical simulation of occulter traverses. The nature of the differences are presumed attributable to overly conservative estimates in that model's parameters, but verification of this across a broader range of mission types and development of alternate ways of calibrating 'q' and 'μ' should be future goals. The author's external occulter simulator must be regarded as a work in progress. Increasing the fidelity of the occulter orbit model, incorporating architecture-specific constraints, and enhancing the algorithm for candidate selection to account for suitable measures of completeness and science utility would be natural extensions of this work. Along with that development, a way to handle sequencing interrupts and replans that accommodate extended-stay characterization visits in the time-line should be implemented in order to simulate more realistic mission profiles and provide science capacity estimates that match different object-of-interest frequency scenarios. New tools to quantify the completeness of the surveys for different scenarios are needed and future development of the simulator should incorporate methods pioneered by other researchers for that evaluation. Enhanced algorithms to compute required station-duration to ensure uniformity of single-visit completeness is needed to enhanced simulator fidelity.

ACKNOWLEDGEMENTS

Support for this work has been provided by Computer Sciences Corporation (CSC). This work was performed under contracts STI-C-01 (P-816) and STI-111271 between CSC and the Space Telescope Science Institute (STScI). The STScI is operated by the Association of Universities for Research in Astronomy, Inc. (AURA) for the National Aeronautics and Space Administration (NASA), under contract with the NASA/Goddard Space Flight Center.

This contribution is for the *Earth Orbital and Planetary Mission Studies* Session #24, AAS/AIAA, Astrodynamics Specialist Conference, organized by the AAS Space Flight Mechanics Committee and the AIAA Astrodynamics Technical Committee held at Mackinac, Michigan, Aug. 18-23, 2007.

The author thanks Alfred B. Schultz, Jesse Leitner (GSFC) and Merle Reinhart (CSC) for extensive comments returned on early drafts of the modeling section of this paper. Appreciation is extended to Helen M. Hart, Mark Kochte (JHU/APL), Wayne Kinzel, and Dorothy Fraquelli (CSC). Special thanks also goes to Robert A. Brown (AURA), for discussions of TPF science requirements, and to many other unnamed individuals who have discussed various aspects of space science mission operations with the author.

NOTATION

a	=	vehicle acceleration (average or constant).
e	=	natural exponential base (~2.71828).
F_{max}	=	maximum thrust.
g	=	gravitation acceleration at earth's surface (~9.8 m/s^2).
I_{sp}	=	specific impulse of fuel/propulsion.
M_{init}	=	initial vehicle mass.
M_{final}	=	final vehicle mass.
M_{p}	=	propellant mass.
μ	=	statistical density of stations required in accessible area.
n	=	number of stations statistically distributed around the sky.
ν	=	average number of visits to each station.
π	=	ratio of a circle circumference and diameter.
q	=	factor < 1 encapsulating restrictions on vehicle travel directions.
T_{thrust}	=	total time spent under acceleration by vehicle.
$T_{1\text{-transit}}$	=	average time of transit between consecutive stations.
$T_{1\text{-station}}$	=	average time spent on station with little propellant use.
$T_{mission}$	=	total duration of mission.
s	=	average distance between stations (linear, not spherical).
z	=	distance between platform and spherically distributed stations.

REFERENCES

1. M. B. Lyot, "A Study of the Solar Corona and Prominences without Eclipses", *Monthly Notices of the Royal Astronomical Society*, v. 99, pp. 579-595, 1939.

2. B. A. Smith and R. J. Terrile, "A circumstellar disk around beta Pictoris", *Science*, v. 226, pp. 1421–1424, December 1984.

3. A. Quierrenbach, ed., "Coronographic Methods for the Detection of Terrestrial Planets", Conclusions from a workshop held at Leiden University, February 02-06, 2004.

4. Lyman Spitzer, "The Beginnings and Future of Space Astronomy", *American Scientist*, v. 50, no. 3, p. 473, September/October, 1962.

5. G. R. Woodcock, in Future Space Transportation Systems Analysis, Appendix to Boeing contract study for NASA, NAS9-14323, December 11, 1974.

6. C. Marchal, "Concept of a space telescope able to see the planets and even the satellites around the nearest stars", *Acta Astronautica*, v. 12, no. 3., pp.195-201, Pergamon Press, 1985.

7. C. J. Copi, G. D. Starkman, 2000, "The Big Occulting Steerable Satellite (BOSS)", *The Astrophysical Journal*, vo1. 532, pp.581-592, March 2000.

8. Robert. A. Brown, C. J. Burrows, S. Casertano, M. Clampin, D. Ebbets, E. B. Ford, K. W. Jucks, N. J. Kasdin, S. Kilston, M. Kuchner, S. Seager, et.al., "The 4-m space telescope for investigating extrasolar Earth-like planets in starlight: TPF is HST2", *Future EUV/UV and Visible Space Astrophysics Missions and Instrumentation*., Proc. Of SPIE, v. 4854, pp. 95-107, eds. J. C. Blades, O. Siegmund, 2003.

9. J. Trauger, "A laboratory demonstration of the capability to image an Earth-like extrasolar planet", *Nature*, v. 446 Issue 7137, pp.771-773, April 2007.

10. W. Cash, C. Copi, S. Heap, N. J. Kasdin, S. Kilston, M. Kuchner, M. Levine, A. Lo, C. Lillie, R. Lyon, R. Polidan, S. Shaklan, G. Starkman, W. Traub, R. Vanderbei, "External Occulters for the Direct Study of Exoplanets", submitted to the ExoPlanet Task Force in Response to the NASA Call for White Papers, April 2, 2007.

11. NASA JPL *Terrestrial Planet Finder Mission Architecture Study Reports*, JPL Publication 02-017 08/09, Electronic Publishing Services, 2002

12. Private communication, 2003/4.

13. W. Cash, E. Schindhelm, J. Arenberg, R. Polidan, S. Kilston, C. Noecker, "The New Worlds Observer: Using Occulters to Directly Observe Planets", *Space Telescopes and Instrumentation I: Optical Infrared and Millimeter*, Proc. of SPIE, v. 6265, ed. J. Mather, H. MacEwen, M. de Graauw, 2006.

14. W. Cash, "Detection of Earth-like planets around nearby stars using a petal-shaped occulter." *Nature*, v.442 pp.51-53, July 6, 2006.

15. R. MacQueen, J. Gosling, E. Hildner, R. Munro, A. Poland, C. Ross, "Initial results from the High Altitude Observatory white light coronagraph on Skylab—A progress report", *Philosophical Transactions of the Royal Society*, Series A. v. 281, no. 1034, pp. 405-414, London, May 6, 1976.

16. A. Bemporad, G. Poletto, J. Raymond, S. Giordano, "A review of the SOHO/UVCS observations of sun grazing comets", *Planetary and Space Science*, v. 55, issue 9, pp. 1021-1030, 2007.

17. W. L. Simmons, W. C. Cash, S. Seager, E. Wilkinson, N. J. Kasdin, R. J. Vanderbei, N. Chow, E. Gralla, and J. Kleingeld, "The New Worlds Observer: a mission for high-resolution spectroscopy of extra-solar terrestrial planets", Proc. of SPIE, *Optical, Infrared, and Millimeter Space Telescopes*, ed. by J. C. Mather, Volume 5487, pp. 1634-1645, 2004.

18. A. B. Schultz, D. Schroeder, et.al., "Imaging planets about other stars with UMBRAS", in *Infrared Space borne Sensing VII*, M. Strojnik, B. Andersen, eds., Proc. of SPIE, v.3759, no. 49, 1999.

19. E.g., URLs: http: //newworlds.colorado.edu , http: //boss.phys.cwru.edu , http: //umbras.org , 2007.

20. C. A. Beichman, N. J. Woolf, C. A. Lindensmith, eds., The Terrestrial Planet Finder. A NASA Origins Program to Search for Habitable Planets, *JPL Pub. 99-3*, May 1999.

21. I. J. E. Jordan, A. B. Schultz, D. Schroeder, "Enhancing NGST Science: UMBRAS", at NGST Science & Technology Exposition, Hyannis, MA, Sep. 13, 1999, *Publications of the Astronomical Society of the Pacific*, CS-207, p. 468, 1999.

22. I. J. E. Jordan, H. M. Hart, G. D. Starkman, et.al., "The advantages of multiple coronographic vehicles in occulter missions", AIAA 2003-6300, *Conf. Proc. Space 2003*, Los Angeles, CA., Sept. 2003.

23. I. Jordan, H. Hart, R. Lyon, A. B. Schultz, G. Starkman, C. Copi, R. Woodruff, et.al., "Relaxing TPF System Requirements with an External Occulter", P-092, Second International TPF-Darwin Conf., San Diego, CA., July 26-29, 2004, http://planetquest1.jpl.nasa.gov/TPFDarwinConf/index.cfm .

24. Amy Lo, Malmstrom, R. Guilmette, T., "New Worlds Observer: Orbit and Sky Coverage", American Astronomical Society Meeting 209, *BAAS* v.38, p.1142, January 2007.

25. S. L. Hunyadi, "TPF-C: Size and Completeness", TPF-C Coronagraph Workshop, JPL, Pasadena, CA, September 28, 2006.

26. Martin Lo, "External Occulter Trajectory Study", TPF-C Coronagraph Workshop, JPL, Pasadena, CA September 29 2006.

27. E. Kolemen & N. J. Kasdin, "Optimal Trajectory Control of an Occulter-Based Planet-Finding Telescope", American Astronautical Society, 07-037, *Proceedings of the AAS Guidance and Control Conference*, Breckenridge, CO, Feb. 3-7, 2007.

28. E. Kolemen, N. J. Kasdin, "Optimal Configuration of a Planet-Finding Mission Consisting of a Telescope and a Constellation of Occulters", American Astronautical Society 07-202, *Proceedings of the AAS Space Flight Mechanics Meeting*, Sedona, AZ, 28 Jan. - 01 Feb., 2007.

29. R. A. Brown, "Expectations for the Early TPF-C Mission", in *Direct Imaging of Exoplanets: Science & Techniques*, Proc. IAU Colloquium no. 200, 2005, ed. C. Aime & F. Vakili, 2006.

30. R. A. Brown, "Obscurational Completeness", *Astrophysical Journal*, v.607, pp. 1003–13, June 1, 2004.

31. R. A. Brown, "Single-Visit Photometric and Obscurational Completeness", *Astrophysical Journal*, v. 624, No. 2, pp. 1010-1024, May 2005.

32. J. Arenberg, "Revisit Times for Exoplanet Searches with a Coronagraph: A Well-aimed Shot in the Dark", *Technology Review Journal,* v. 13, no. 2, pp. 43-62, Northrup Grumman Space Technologies, ed. L. Brekka, Fall/Winter 2005.

33. S. L. Hunyadi, S. B. Shaklan, R. A. Brown, "Optimization of the Terrestrial Planet Finder Coronagraph Program Completeness", *Bulletin of the American Astronomical Society*, Dec. 2005, v. 37, p.1358, American Astronomical Society Meeting 207, Jan. 2006.

34. Steven H. Pravdo, Stuart Shaklan, R. A. Brown, S. L. Hunyadi, "Observation Strategies and Statistics of TPF and Other Planetary Observations", Amer. Astronomical Soc. Meeting # 210, May 2007.

35. I. J. E. Jordan, "Planning and Scheduling External Occulter Space Missions", *Proc. from the 5th International Workshop on Planning and Scheduling for Space*, Baltimore, MD, October 22-25, 2006.

36. M. D. Rayman, S. N. Williams, "Design of the First Interplanetary Solar Electric Propulsion Mission", *Journal of Spacecraft and Rockets*, AIAA, v.39, no. 4, July-August 2002.

37. R. A. Brown, "Chasing Earth-like planets", *STScI Annual Report*, for 2005, pp. 24-26, 2006.

38. I. Jordan, A. Schultz, H. Hart, F. Bruhweiler, D. Fraquelli, F. Hamilton, J. Hershey, "UMBRAS: Design of a Free-Flying Occulter for Space Telescopes", AIAA 2000-5230, *Proc. Space 2000 Conference*, Long Beach, CA, Sept. 19, 2000.